No-contact GPR for investigating painted walls

No-contact GPR for investigating painted walls

Massimiliano Pieraccini, Lapo Miccinesi
Department of Information Engineering
University of Florence
Via Santa Marta, 3 50139 Firenze, Italy
massimiliano.pieraccini@unifi.it

***Abstract*—In this paper a no-contact ground penetrating radar for investigating painted walls is presented. It operates at 10 GHz central frequency with 4 GHz bandwidth. Its mechanical positioner is able to scan a surface 1.4 m wide and 1.9 m high. This equipment has been specifically designed for investigating the painted walls of the Tutankhamon tomb in the Kings' valley in Egypt. The aim of this radar survey is to gather information about the shallow layers (the plaster and the existence of possible plaster voids affecting the future stability of paintings) up to 0.5 m depth.**

Keywords—archaelogy; cultural heritage; ground penetrating radar, masonry, mural painting.

I. INTRODUCTION

Ground Penetrating Radar (GPR) is commonly used for investigating masonry/stone walls [1], [2], [3]. Most GPR systems operate at low frequency and in contact with the surface under investigation. Nevertheless, there are some special applications for which these constrains are not effective. Investigation of ancient painted walls is one of these. Indeed, the contact with these painted surfaces should be avoided as much as possible, the image resolution should be as high as possible (ideally in the order of some centimeters) for gathering information about the plaster and possible detachment. Therefore it could be necessary a radar operating at distance, at high frequency and with large bandwidth. In standard applications, the high frequency is avoided because of high attenuation (the attenuation coefficient is roughly proportional to frequency), but in the investigation of painted walls the measurement time rarely is a constraint, so the high attenuation can be compensated by a very long integration time.

In 2002 one of the authors of this paper developed a no contact high frequency radar for masonry investigation [4],[5]. That equipment was specifically designed for investigating the ancient walls of the "Salone dei cinquencento" (Hall of 500s) in the City Hall of Florence (Italy) [6]. The aim was to search a lost fresco of Leonardo Da Vinci, that some scholars thought to be behind one of these walls. As the painted surface was very large (over 400 m^2), the radar scanned vertical lines 3 meter long differently spaced (between 0.5 m and 2 m). So it was not able to provide three-dimensional images of the wall structure.

This paper presents a no-contact high frequency radar for wall investigation entirely redesigned with 3D imaging capability. It performs horizontal and vertical movements scanning a surface 1.4 m wide and 1.9 m high. The gathered data are focused with a back-propagation algorithm that takes into account of the Snell's law on the interface between air and wall.

This radar has been specifically designed for investigating the painted walls of the Tutankhamon tomb in the Kings' valley in Egypt (see Figure 1 and Figure 2).

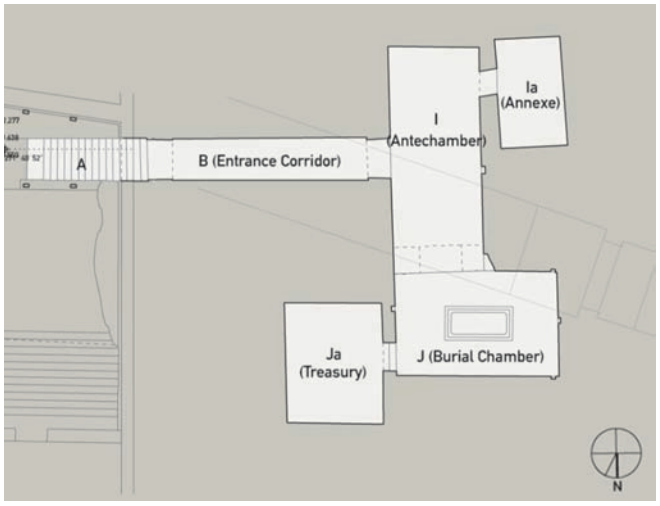

Figure 1. Map of Tutankhamon tomb [7]

Figure 2. Painted walls of the Burial Chamber of Tutankhamon tomb [7]

The Tutankamon tomb has already been investigated using GPR. In 2015, Nicholas Reeves [7] argued that behind the walls of Tutankamon tomb there was the access to Nefertiti's chamber (the queen mother of Tutankamon). In the November of the same year Hirokatsu Watanebe scanned the tomb's walls with a 400 MHz GPR. Its final report [8] show very noised images without any calibration and without scale. Nevertheless he states to be able to confirm the hypothesis of Reeves. Other GPR investigations conducted by independent researchers [9],[10],[11] denied the findings of Watanebe. At the state of art there is not evidence of buried chambers or cavities behind the walls of Tutankhamun tomb, while there are convincing

978-1-5386-5777-5/18/$31.00 ©2018 IEEE

clues, based on GPR images, that there is not other chambers or cavities in the Tutankhamun tomb.

All these GPR investigations have been aimed to find a large chamber/cavity as proposed by Reeves, but a systematic radar survey of the painted surfaces has never performed. It could be give valuable information about the plaster and the existence of possible plaster voids affecting the future stability of paintings. The aim of the radar described in this paper is just to gather this kind of information up a depth of 0.5 m.

II. The Radar Equipment

The radar equipment is sketched in Figure 3. The mechanical frame is positioned in front of the wall under investigation and it scans 1.4 m in the horizontal axis and 1.9 m in vertical axis. Two step-by-step motors controlled by the acquisition software move the radar head. The radar operates a Step Frequency Continuous Wave (SFCW) modulation. The central frequency is 10 GHz. The bandwidth is 4 GHz. A Vector Network Analyzer (HP 8720A) operates as transceiver.

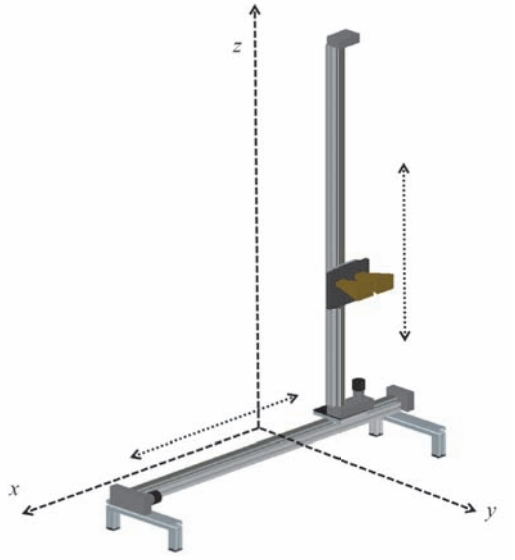

Figure 3. Sketch of the radar equipment

With reference to Figure 4, the VNA output power is -13 dBm. The first TX amplifier with 12 dB gain increases the power to -1 dBm. A -3 dB attenuator reduces the power to -4 dBm. The one-way cable loss is -5 dB, so the input power of the second TX amplifier is - 9 dBm. The gain of the second TX amplifier is 28 dB. Its output compression point is 19 dBm, so the input power has to be lower than -9 dBm, as indeed it is. Two single-pole double-throw (SPDT) switches provide a direct path (through a 40 dB attenuator) between the transmitter and the receiver in order to perform calibrated measurements. The insertion loss of each SPDT is negligible. So the power in TX antenna is 19 dBm. When the signal passes through the calibration path, the input power of the RX amplifier results -21 dBm. The gain of the first RX amplifier is 28 dB (Output compression point: 19 dBm, Noise Figure: 5 dB). The cable attenuation is -5dB, so the signal at the RX channel of VNA is 2 dBm in calibration.

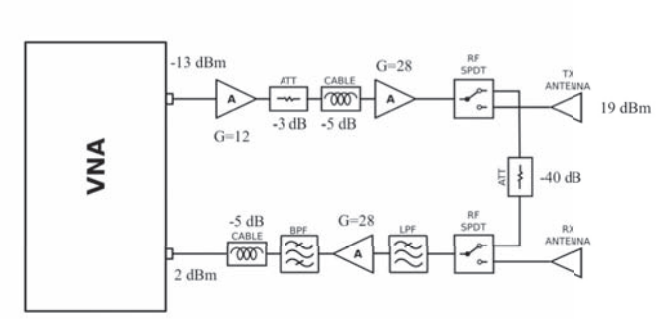

Figure 4. Block scheme of radar

The power during the measurement depends on the distance between the antenna and the wall. For a distance of 1.62 m, the signal acquired by RX antenna is about -40 dB the signal transmitted by TX antenna. Therefore the powers in the RX channel of VNA in measurement and in calibration are about equal. As general rule, the attenuation in calibration path should be set in order to obtain about the same power in calibration and measurement.

III. The Focussing Algorithm

The acquired raw data have been focused by using a back-projection algorithm that takes into account the electromagnetic path between the antennas and any image point [4], [6]. With reference to Figure 5:

$$d_1 = \sqrt{(x_A - x_S)^2 + (y_A - y_S)^2 + (z_A - z_S)^2}$$
$$d_2 = \sqrt{(x_S - x_P)^2 + (y_S - y_P)^2 + (z_S - z_P)^2} \quad (1)$$

Where (x_A, y_A, z_A) is the antennas' position, (x_P, y_P, z_P) is the image point, (x_S, y_S, z_S) is the point where the electromagnetic path from antenna to image point intercepts the surface between the two media. The coordinates (x_S, y_S, z_S) can be estimated using the Fermat's principle (i.e. the least time principle). The travel time between antennas and image point is $t=t_1+t_2$, where t_1 and t_2 are the travel time respectively in the first and second medium:

$$t_1 = \frac{c}{\sqrt{\varepsilon_1}} \qquad t_2 = \frac{c}{\sqrt{\varepsilon_2}} \quad (2)$$

For a given antennas' position (x_A, y_A, z_A) and for a given image point (x_P, y_P, z_P), t depends only on the coordinates x_S and z_S. Therefore, it is possible to evaluate the distance d, by searching the minimum of t in function of x_S and z_S.

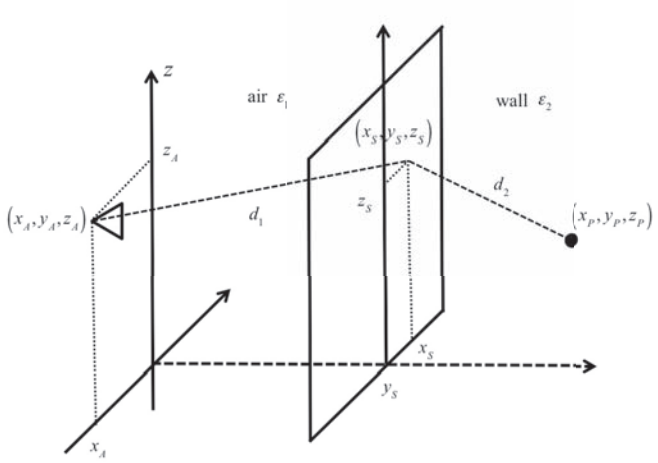

Figure 5. Geometry of the focusing algorithm

In the specific application the first medium is air, the second medium is the wall under investigation. The distance between the antenna plane ($y = 0$) and the wall ($y = y_S$) has to be large enough to avoid that the multiple reflections between antenna and wall cover the signal inside the wall. In practice, if we assume $\varepsilon_2 \cong 4$, the maximum investigation depth inside the wall is twice the distance (y_S) between antenna and wall.

IV. Experimental Tests

The first experimental session with the radar equipment was aimed to assess its dynamic. As it is known, the penetration depth depends on clutter free dynamic range [12].

Figure 6 shows the IFFT of the acquired signals. The red line is the IFFT in calibration, i.e. when the RF signal passes through the calibration path instead of the antennas. The green line is the IFFT in measurement, i.e. when the signal passes through the antennas pointed at a wall at 1.6 m distance. A padding factor of 50 and a Kaiser window with β=10 have been applied to raw data in frequency domain, before the calculation of IFFT.

The red peak labeled with A is the signal transmitted through the calibration path ("cable"). The red peaks B and C are the harmonics of the main peak (A) that are low but not totally negligible. The peak labeled with D in the green plot is the coupling between the antennas, while the peak labeled with E is the signal back reflected by the wall. The peak labeled with F is the double reflection of the signal back reflected by the wall (i.e. reflected by the wall, by the antennas, and again by the wall).

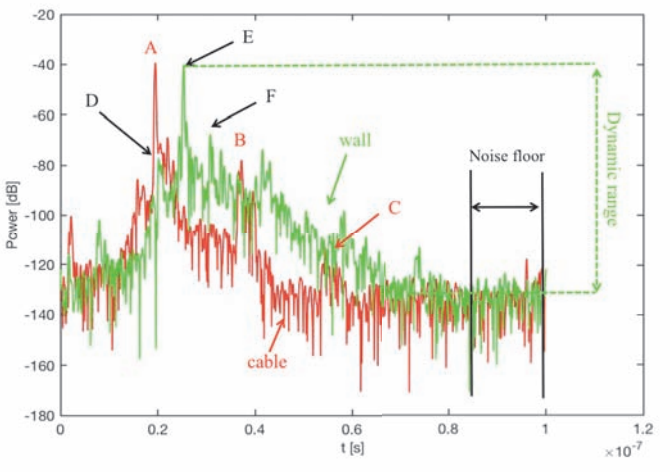

Figure 6. Calibration (red line) and measurement (green line)

Figure 7 shows the dynamic range of the signal through the calibration path ("cable") and the signal acquired through the antennas pointed at the wall ("wall"). The measurement has been carried out range with IF bandwidth of 100 Hz. The dynamic range is calculated as ratio between the highest peak and the noise floor (calculated as average between 25 m and 28 m of the time plot). By averaging subsequent acquisitions the noise floor decreases until to its least value. In theory this value should depend only on the effective dynamic range of VNA. The declared dynamic range of VNA is 95 dB with a single measure at IF= 100 Hz. The plot in Figure 7 shows that for N=1 the dynamic range is 94 dB for cable and 91.6 dB for the wall. These values are in agreement with the specification of VNA. Furthermore by increasing the number of acquisitions, as expected, the dynamic range increase up to the maximum value that is related to the effective number of bits (ENOB) of Analog/Digital Converter. We observe that dynamic range is about 4.5 dB lower when the signal passes through the antennas than when the signal passes only through the calibration path.

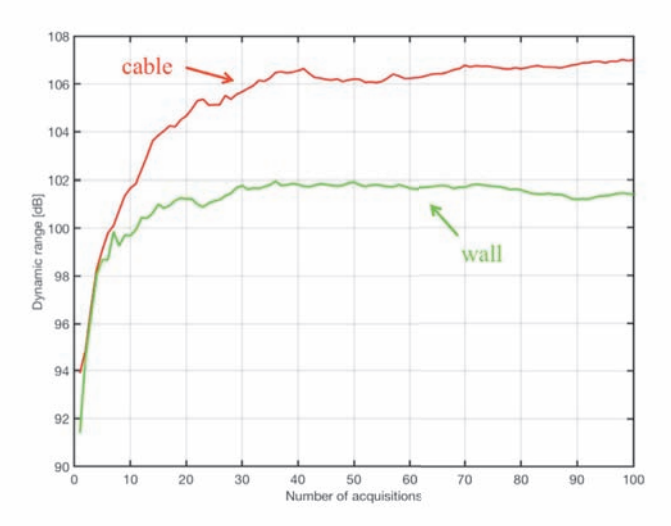

Figure 7. Dynamic range in calibration (red line) and in measurement (green line)

After these preliminary measurements, the radar scanned a vertical surface 1.4 m large and 1.9 m high at step of 15 mm. The number of step along x was $N_x = 93$, the number of steps along z was $N_z = 126$, the number of frequencies was $N_f = 801$, the duration of each single tone was 10 ms. Therefore the whole integration time (t_{int}) can be calculated as

$$t_{\text{int}} = N_x N_z N_f t_{tone} = 23.3 \text{ hours} \quad (3)$$

On the other hand the effective measurement time (t_{meas}) inclusive of movement times was 38.8 hours. Therefore the duty cycle of this equipment has been 60.0 %.

The equipment has been tested on a masonry wall of 42 cm of thickness. The relative dielectric constant of the wall, was measured with a free-space technique [13] and results $\varepsilon_2 = 3.9$.

Figure 8 shows the IFFT of the horizontal scan at z = 0.95 m. The time axis is reported in range (by supposing the speed of the electromagnetic waves equal to the speed of light in vacuum). At $y_1 \approx 1.7$ m is possible to see the signal due to the first reflection on the entrance surface of the wall. The signal from the exit surface is well visible at $y_2 \approx 2.5$ m, indeed $(y_2 - y_1)/\varepsilon_2^{1/2} \approx 0.41$ m. Therefore the radar signal is able to penetrate the whole thickness of the wall. The signal at about 3.5 m range is clearly the double reflection between the radar and the wall.

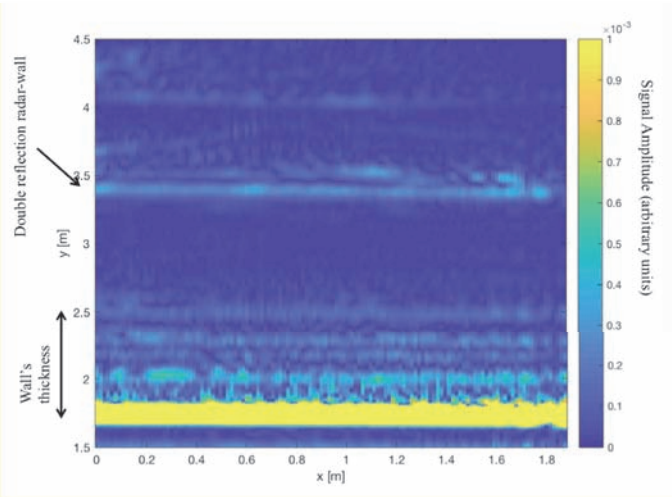

Figure 8. IFFT of the horizontal scan at z = 0.95 m

Figure 9 shows the power image focused on the wall's surface (at y =1.62 m). As the electromagnetic path is completely in the same medium (air), it was not necessary to apply the Snell's low.

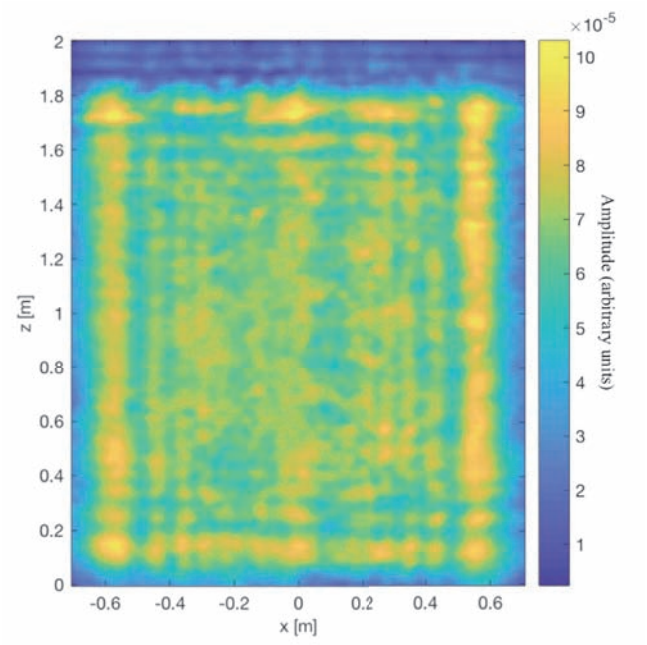

Figure 9. Power image focused on the wall's surface (y=1.62 m)

It is possible to note the difference consistence of the plaster on the wall surface. Figure 10 shows the phase of the same radar image in Figure 9. This image gives information about the planarity of the wall. It is interesting to note the horizontal discontinuity at z=1.9 m given by an external plastic electrical conduit (see Figure 11).

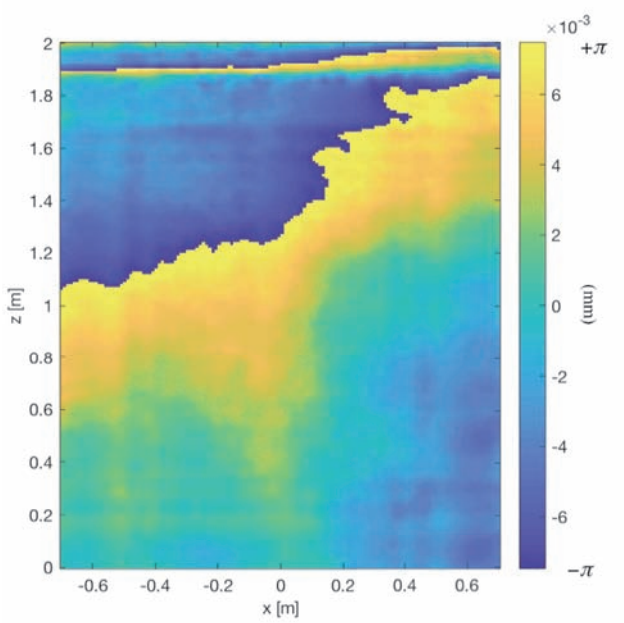

Figure 10. Phase image focused on the wall's surface (y=1.62 m)

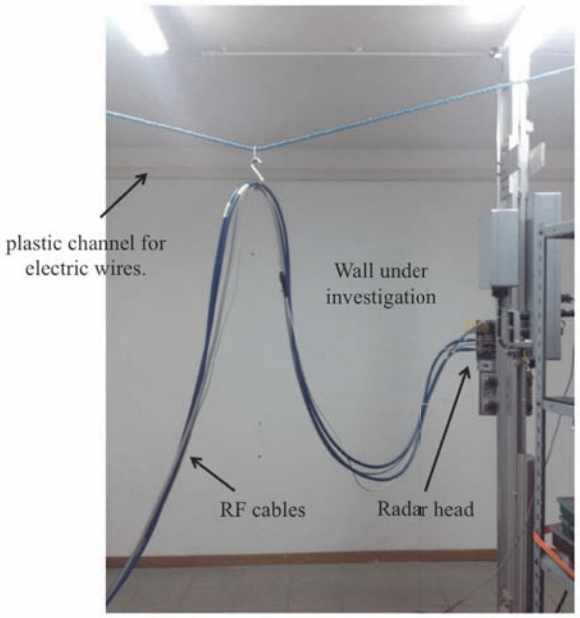

Figure 11. Picture of the wall under investigation

Figure 12 shows the power image focused on a vertical plane at y = 1.82 m (20 cm inside the wall).

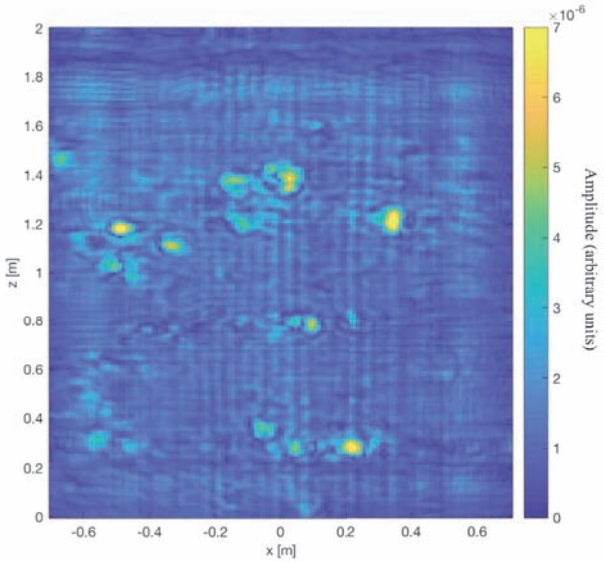

Figure 12. Power image focused on a vertical plane 20 cm inside the wall

Figure 13 shows the power image focused on a vertical plane at y = 2.02 m (40 cm inside the wall, i.e. on the backside surface of the wall). The horizontal lines at z = 0.3 and at z = 1.3 m are electrical conduits embedded in the wall masonry.

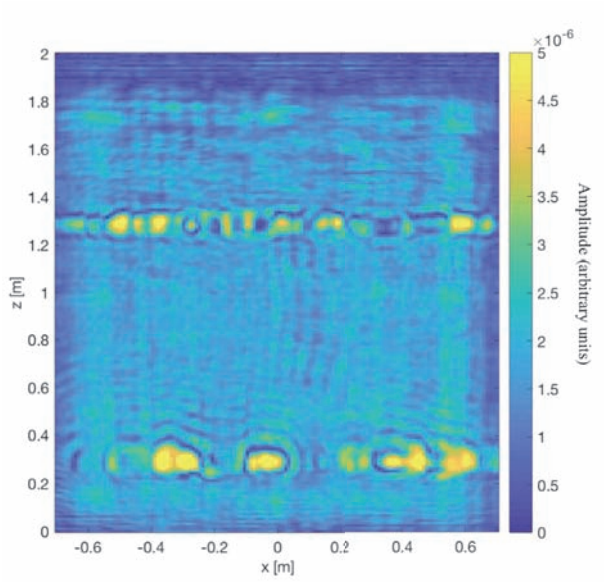

Figure 13. Power image focused on a vertical plane 40 cm inside the wall

V. Conclusion

A high frequency large bandwidth GPR scanner for wall investigation has been designed and successfully tested on a test wall. The attenuation at high frequency is compensated with a suitable long acquisition time. It is important to note that the double reflection between radar and wall limits the penetration depth, so the depth of interest should be no more then a half of the distance between radar and wall. The radar has been demonstrated to be able to detect target inside a wall such as buried electrical conduit or small imperfections. Finally we note that the interferogram focused on the surface of the wall gives information on its planarity and it could be used for improving the focusing algorithm by taking into account the effective 3D shape of the wall surface.

References

[1] Ch. Maierhofer, S. Leipold. “Radar investigation of masonry structures.” NDT & E International, Vol. 34, No. 2, pp. 139-157, March 2001

[2] C. Colla, A. J. Fernàndez, S. Garanzini, M. Marelli, “Diagnostic by imaging: 3D GPR investigation of brick masonry and post-tensioned concrete.” 13th International Conference on Ground Penetrating Radar (GPR2010), June 2010

[3] S. Santos-Assunçao, V. Perez-Gracia, O. Caselles, J. Clapes, V. Salinas V. “Assessment of complex masonry structures with GPR compared to other non-destructive testing studies.” *Remote Sensing*, Vol. 6, No. 9, pp. 8220-8237, August 2014

[4] M. Pieraccini, G. Luzi, D. Mecatti, L. Noferini, C. Atzeni, “High-frequency penetrating radar for masonry investigation.” Ninth International Conference on Ground Penetrating Radar. Vol. 4758. International Society for Optics and Photonics, 2002.

[5] M. Pieraccini, G. Luzi, L. Noferini, D. Mecatti, C. Atzeni, C. “Joint time-frequency analysis for investigation of layered masonry structures using penetrating radar.” *IEEE transactions on geoscience and remote sensing*, Vol. 42, No. 2, pp. 309-317, Febbruary 2004

[6] M. Pieraccini, D. Mecatti, G. Luzi, M. Seracini, G. Pinelli, C. Atzeni, “Non-contact intrawall penetrating radar for heritage survey: the search

of the 'Battle of Anghiari' by Leonardo da Vinci." NDT & E International, Vol. 38, No. 2, pp. 151-157, March 2005

[7] Reeves, N. "The Burial of Nefertiti?" Amarna Royal Tombs Project, Occasional Paper No. 1 July 2015

[8] Watanabe H., Report on the radar survey of the tomb of Tutankhamun (KV 62) 26-27 November 2015 (traslated by Shohta Ueno and Alexandra J. Park)

[9] Report of Dr. Dean Goodman (Geophyisical Archaeometry Laboratory)

[10] Report of Glen Dash (The Glen Dash Institute)

[11] Report of Dr. Margaret Watters (US National Park Service)

[12] S. E. Hamran, "Radar performance of ultra wideband waveforms," in Radar Technology, G. Kouemou, Ed. Rijeka, Croatia: InTech, 2010. [Online]. Available: http://www.intechopen.com/books/radar-technology/radar-performance-of-ultra-wideband-waveforms

[13] D. K. Ghodgaonkar, V. V. Varadan, V. K. Varadan, "A free-space method for measurement of dielectric constants and loss tangents at microwave frequencies." IEEE Transactions on Instrumentation and measurement, Vol. 38, No. 3, pp. 789-793, June 1989